Journal of the Optical Society of Korea
Vol. 14, No. 3, September 2010, pp. 266-276

DOI: 10.3807/JOSK.2010.14.3.266

Optical System with 4 μm Resolution for Maskless Lithography Using Digital Micromirror Device

Dong-Hee Lee*

Department of Optometry, Eulji University, Seongnam 461-713, Korea

(Received August 2, 2010 : revised August 26, 2010 : accepted August 27, 2010)

In the present study, an optical system is proposed for maskless lithography using a digital micromirror device (DMD). The system consists of an illumination optical system, a DMD, and a projection lens system. The illumination optical system, developed for 95% uniformity, is composed of fly's eye lens plates, a 405 nm narrow band pass filter (NBPF), condensing lenses, a field lens and a 250W halogen lamp. The projection lens system, composed of 8 optical elements, is developed for 4 μm resolution. The proposed system plays a role of an optical engine for PCB and/or FPD maskless lithography. Furthermore, many problems arising from the presence of masks in a conventional lithography system, such as expense and time in fabricating the masks, contamination by masks, disposal of masks, and the alignment of masks, may be solved by the proposed system. The proposed system is verified by lithography experiments which produce a line pattern with the resolution of 4 μm line width.

Keywords : Projection lens, Lens design, Aberration, Maskless lithography, Resolution
OCIS codes : (220.0220) Optical design and fabrication; (080.1010) Aberration theory; (080.3620) Lens design; (110.3960) Microlithography

I. INTRODUCTION

Conventional lithography using a mask was invented in the 18th century. Even now, most of the lithography carried out uses masks. Due to the problems caused by masks such as expense and time in fabricating the masks, contamination by masks, disposal of masks, and the alignment of masks, research on maskless lithography was initiated.

Recently, Spatial Light Modulator (SLM) devices for Micro Electro Mechanical System-based (MEMS-based) digital light processing have brought innovation to the microdisplay field. These SLM devices include the Digital Micromirror Device (DMD) by Texas Instruments Inc. and some other SLMs) [1-5]. Nowadays, many new application fields for them have emerged. One of them is maskless lithography for semiconductor and Flat Panel Display (FPD) fabrication [3-10].

In the maskless lithography described in this paper, the micromirror array works like a mask to write patterns directly onto substrates. In comparison with other maskless lithography technologies, the micromirror based lithography technology possesses superior features. It is characterized by sufficient throughput for highly customized patterns, fine lithographic quality, efficiency in cost and time [9], and so on. Nevertheless, the micromirror based lithography is feasible if, and only if, each system developer could set up an excellent optic unit [10, 11], and an accurate DMD control unit [3-8, 12]. To fabricate lithographic patterns, millions of micromirrors on the DMD need to be addressed and adjusted, individually and instantaneously. However, detailed discussion on the DMD control is beyond the scope of this paper. The details on the DMD control associated with the proposed system can be found in the literature [8, 12].

Due to increasing demands for small electronics, the Printed Circuit Board (PCB) circuit pattern size has been decreased gradually and is now down to 10 μm. Therefore, the optical system [12] developed for Plasma Display Panel (PDP) fabrication which has 30 μm resolution can not be used for PCB fabrication. A new optical system is needed. This study is focused on the development of a 4 μm resolution optical system for high resolution maskless lithography using the DMD for PCB fabrication.

*Corresponding author: dhlee@eulji.ac.kr
Color versions of one or more of the figures in this paper are available online.

II. DESIGN OF OPTICAL SYSTEM FOR MASKLESS LITHOGRAPHY

The proposed system consists of an illumination optical system, a DMD, and a projection lens system. The illumination optical system composed of fly's eye lens plates, a 405 nm NBPF, condensing lenses, a field lens and a 250W halogen lamp is developed to achieve 95% uniformity. The projection lens system, composed of 8 optical elements, is developed for 4 μm resolution.

2.1. Design of illumination optical system

Success of the design for an illumination optical system depends on two design strategies; one is to achieve the high uniformity of the illumination beams on the DMD surface and the other is to achieve the complete incidence of all the illumination beams reflected from the DMD surface upon the effective aperture of the projection lens. For uniform illumination on the DMD surface, we designed a beam homogenizer using fly's eye lens plates, and for the illumination beams to be incident upon the effective aperture of projection lens, we properly adjusted the distance between the first and second fly's eye lens plate, the curvature radius of the unit cell of the fly's eye lens, and the focal length of the subsequently arranged field lens.

In the design, we used a 250W halogen lamp supplied by USHIO Co. and we used a NBPF to utilize the line width of 405nm ±2 nm. As to the reflector of the lamp, we used only the 47.4 mm depth section ranging from one end of the major axis of an ellipsoid with major axis of 252 mm and minor axis of 128 mm. The inner surface of the reflector was coated to be a cold coating mirror at 350~480 nm wavelength. As a result, according to the simulation, the illumination beams reflected from the lamp were collected on the focus with about ±15° angle of convergence. Then we let the collected illumination beams pass through a variable diaphragm which acts as a pinhole with a 3~5 mm diameter. To make these illumination beams uniformly illuminate the DMD surface and to let all of them again enter into the effective aperture of projection lens, we let all of them pass through a beam homogenizer consisted of condensing lenses, two fly's eye lens plates, and a field lens. A configuration of the initial design of the homogenizer is given in Fig. 1.

If the cell width of the fly's eye lens is d, the focal distance of field lens, f_3', the focal distance of the second fly's eye lens, f_2', and the width needed for uniform illumination, D, the following formula is established.

$$d = \frac{f_2'}{f_3'} D \tag{1}$$

Where, f_2' is equivalent to the width between two fly's eye lens plates.

As specified in Table 1, the tilting angle of the micro-

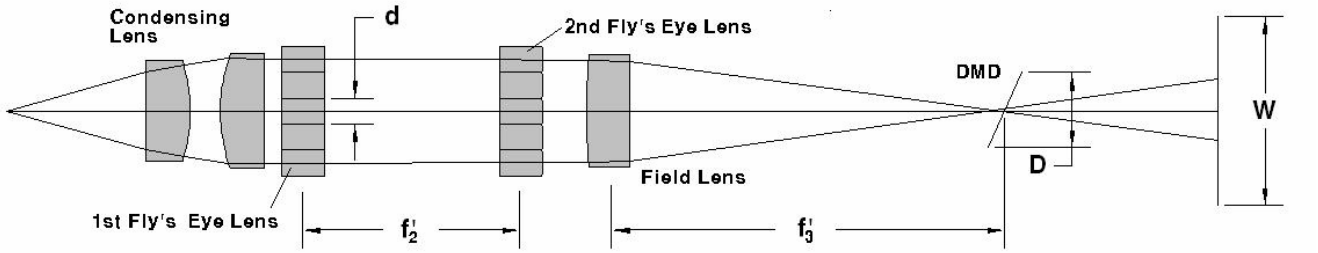

FIG. 1. Configuration for the initial design of homogenizer.

TABLE 1. Optical and physical parameters of DMD(quoted from DMD 0.7 XGA LVDS DMD Discovery™ Product Preview)

Parameter.	Min	Nom	Max	Unit
Mirror Tilt − half angle (Variation device to device)	11	12	13	Degrees
Axis of Rotation − Lower Right to Upper Left (Variation device to device)	44	45	46	Degrees
Mirror Metal Specular Reflectivity (420nm − 700nm)		89.4		%
DMD Efficiency (420nm − 700nm)		68		%
Number of Columns		1024		
Number of Rows		768		
Mirror (Pixel) Pitch		13.68		um
Total Width of Active Mirror Array(1024 pixels)		14.008		mm
Total Height of Active Mirror Array(768 pixels)		10.506		mm

mirror is 12° and, thus, the projection lens can be placed vertically against the horizontally positioned homogenizer only when the DMD surface is tilted against the optical axis of the illumination beams at an angle of 66°. Given that the effective diagonal size of DMD is 17.51 mm (calculated from the parameters of DMD in Table 1), the optimum area needed for homogenous illumination is the elliptical shape with long axis of 17.51 mm and short axis of 16 mm(=17.51×cos24°). Considering factors such as assembling tolerance of the homogenizer, there is a need to extend the uniform illumination area to about 18 mm in the initial design. Therefore, if we let D be 18.00 mm, f_3' be 250 mm from the field lens to the DMD, and the cell width of the fly's eye lens be 4 mm, in Eq. (1), the distance between two fly's eye lens plates becomes f_2' = 55.56 mm.

Based on these, Table 2 and Fig. 2 show the optimized design data and configurations taking into account the actual thickness of lenses. As depicted in Fig. 2, the illumination beams starting from the lamp pass through a 3 mm diaphragm and fly's eye lens plates almost in parallel by means of two condenser lenses. Fig. 2(a) shows ray tracings of the illumination beams that radiate from the center of the diaphragm at an angle of ±15°. It shows the illumination beams going through a cross section made up of a 49-element fly's eye lens plate, of which the cell dimension is 4 mm in height, 4 mm in width, and 8 mm in depth, passing through the homogenizer and the effective size of the DMD, and entering into the effective diameter of the projection lens. Fig. 2(b) shows that the illumination beams, which radiate from the edge of the 3 mm diaphragm, pass through the homogenizer and the effective size of the DMD, and are able to enter into the effective diameter of the projection lens. If the illumination beams fail to pass through the real DMD size, they won't be reflected by the micromirror of the DMD and thus cannot be incident upon the projection lens. Hence, in Fig. 2(a) and (b), the rays of illumination beams not passing through the real DMD size (14.008 mm × 10.506 mm from Table 1.) can't be reflected toward the projection

TABLE 2. Data of the optimized homogenizer

Surface	Radius(mm)	Thickness(mm)	Remark
diaphragm	Infinity	32.0	
2	Infinity	10.0	Fused Silica
3	-40.5	7.0	
4	40.5	10.0	Fused Silica
5	Infinity	14.0	
6	23	8.0	7x7 elements of fly's eye lens (WxHxD:4.0x4.0x8.0) Fused Silica
7	Infinity	38.0	
8	Infinity	8.0	7x7 elements of fly's eye lens (WxHxD:4.0x4.0x8.0) Fused Silica
9	-23	10.0	
10	125	10.0	Fused Silica
11	Infinity	120.0	
12	Infinity	140.0	Cold Mirror
13	Infinity	260.0	DMD
14	Infinity	0.0	Projection Lens

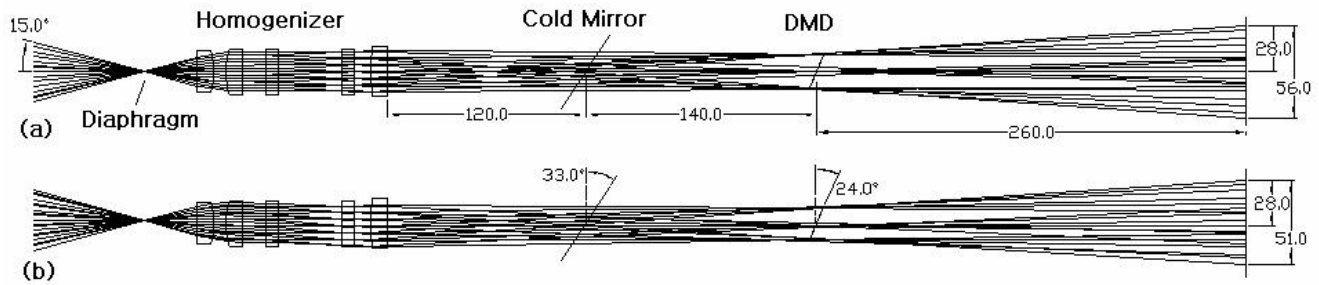

FIG. 2. Configuration showing ray tracings of the illumination beams in the optimized homogenizer.((a): ray tracings for the illumination beams that radiate from the center of the diaphragm at an angle of ±15°; (b): ray tracings for the illumination beams that radiate from the edge of the 3 mm diaphragm at an angle of ±15°)

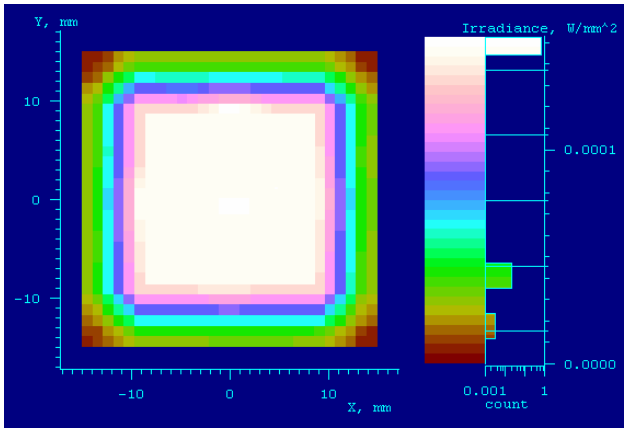

FIG. 3. Simulation results for the distribution of the illumination beams on DMD by the optimized homogenizer (simulated by Light Tools S/W).

lens and, therefore, do not need to be taken into account when calculating an effective aperture of the projection lens. Finally, by real ray tracings, we could confirm that the illumination beams, which are to pass through the real DMD size and be incident upon the projection lens, are within 52 mm of the projection lens in diameter, which implies that the effective diameter of the projection lens should be 52 mm or more. Also, this implies that the initial paraxial marginal ray angle should be $\frac{52}{2\times 260}=0.1rad$ and the object numerical aperture (NA) is 0.1, which should be used in the next section. Fig. 3 shows the simulation results of the illumination beam distribution by the designed illumination optical system at the position of the DMD. We conclude that 95% or more uniformity can be achieved in the area of 18 mm×18 mm.

2.2. Design of projection lens system

Among the objective lenses for projection, the Biotar (DoubleGauss) type is used widely because the optical properties of meniscus lenses which are presented symmetrically inside the system are superior to lenses of other types. Thus, many high-performance lenses are designed by adopting a variant of this type. Also, we would like to find the numerical solutions of the initial design by adopting the Biotar (DoubleGauss) type [13]. However, in the DMD projection optics, because the NBPF passes only the light of a narrow band of 450 nm±2 nm wavelength, chromatic aberrations are not important. In the process of determining the initial solution, therefore, we did not need to consider the chromatic aberrations and use only unique index of refraction in order to determine the initial solution promptly. (Actually, we use only FD8 as lens material.)

Finally, in using the Biotar type design, we could isolate the cemented lenses in order to have more degrees of freedom which provide more favorable conditions to find the initial solutions.

Thus, the initial design conditions appropriate to our maskless optical system could be set down as follows:

1) The DMD composed of 1024×768 pixel in which the unit cell size is 13.68 μm×13.68 μm has the overall size of 14.008 mm×10.506 mm. So, in order to make a unit cell image of 4.0 μm×4.0 μm in the substrate, the magnification(m_β) should be -0.2924x.
2) All five kinds of the third-order aberrations should be zero.
3) The telecentricity in image space should be zero.
4) Considering the placement and the space of the homogenizer and the illumination reflection mirror of the DMD optical system which let the illumination beams go toward the DMD, the distance from the DMD plane to the first surface of the projection lens should be 260 mm.
5) The distance from the first surface to the last surface of the projection lens should be less than 140 mm.
6) The working distance from the substrate should be at least 30 mm.

In order to create a computer program to obtain initial solutions, we can summarize the above initial designing conditions as follows using the analytical formulas.

$$m_\beta=-0.2924 \tag{2}$$

$$u_k^{pr}=0 \tag{3}$$

$$S_I=\sum_{i=1}^{k}A_i^2h_i\Delta\left(\frac{u}{n}\right)_i=\sum_{i=1}^{k}I_i=0 \tag{4}$$

$$S_{II}=\sum_{i=1}^{k}A_iB_ih_i\Delta\left(\frac{u}{n}\right)_i=\sum_{i=1}^{k}II_i=0 \tag{5}$$

$$S_{III}=\sum_{i=1}^{k}B_i^2h_i\Delta\left(\frac{u}{n}\right)_i=\sum_{i=1}^{k}III_i=0 \tag{6}$$

$$S_{IV}=H^2\sum_{i=1}^{k}P_i=0 \tag{7}$$

$$S_V=\sum_{i=1}^{k}\frac{B_i}{A_i}(H^2P_i+III_i)=0 \tag{8}$$

$$d_0=260 \tag{9}$$

$$d_i\leq 30 \tag{10}$$

(For 6 elements, l=13; for 7 elements, l=15; for 8 elements, l=17)

$$\sum_{i=1stlens}^{lastlens}d_i\leq 140 \tag{11}$$

$$T_I=\sum_{i=1}^{k}\left({}^5I_i+6I_i\sum_{p=1}^{i-1}{}^5V_p-6II_i\sum_{p=1}^{i-1}I_p\right) \tag{12}$$

Where,

$${}^5I_i=3I_i[c_ih_i(c_ih_i-2u_i)-A_i\Delta\left(\frac{u}{n}\right)_i]$$

$$^5V_i = A_i^2 h_i \Delta(\frac{u^{pr}}{n})_i - A_i \Delta(\frac{u}{n})_i$$

$$\Delta(\frac{u}{n})_i = \frac{u_i}{n_i} - \frac{u_{i-1}}{n_{i-1}}$$

$$\Delta(\frac{u^{pr}}{n})_i = \frac{u_i^{pr}}{n_i} - \frac{u_{i-1}^{pr}}{n_{i-1}}$$

$$P_i = -c_i \Delta(\frac{1}{n})_i$$

$$A_i = n_i(c_i h_i - u_i)$$

$$B_i = n_i(c_i h_i^{pr} - u_i^{pr})$$

$$H = B_i h_i - A_i h_i^{pr}$$

In these equations, c_i is the curvature of surfaces, d_i is the distance between surfaces, u_i is the paraxial marginal ray angle, u_i^{pr} is the paraxial chief ray angle, h_i is the paraxial marginal ray height, and h_i^{pr} is the paraxial chief ray height.

The schematic diagram of the DMD projection system is shown in Fig. 4(a). We want the solutions which are free from all third-order aberrations (S_i=0, i=*I*, *II*, *III*, *IV*, and *V*))[14, 15] with some other constraints.

But the value of the fifth-order spherical aberration (Eq. 12) is only used to compare the initial solutions. In other words, by comparing the value of the fifth-order spherical aberration and by selecting the solution with a smaller value, we can choose the solution with a good condition for optimization.

The above fifth-order spherical aberration is Matsui's expression. Because Matsui's expression [16, 17] is more compact than Buchdahl's [18], we prefer to use his expression. Then, in using Matsui's expression, we should give any restrictions to u_0 and u_0^{pr} (the cases of i=0 in u_i and u_i^{rp}). u_0 is the initial paraxial angle of the ray from the axial object point passing at the height of 1(i.e. in Fig. 4(b), R=1) on the first principal plane, and u_0^{pr} is the paraxial angle made by the principal ray which leaves at the object at the height η defined by the condition that the tangent of the object half-field angle ($\tan\omega = \frac{\eta}{OH}$), viewed from the first principal point, is 1 as shown in Fig. 4(b) [16, 17]. These conditions for u_0 and u_0^{pr} derived from the conditions of R=1 and ω=1 shown in Fig. 4(b) are needed to obtain the fifth-order spherical aberration. The Helmholtz-Lagrange invariant is then -1.

Therefore, the desired initial solutions of the DMD projection system should satisfy the Eqs. (2)~(9) and the restrictions of (10) and (11).

For a system made up of 8 elements, there is a total of 35 variables (i=1~17 for c_i, i=1~18 for d_i). And, for a system made up of 7 or 6 elements, there shall be a total of 31 or 27 variables. Other restrictive conditions with the exception of Eqs. (9)~(11) include 2 mm or more of thickness of the lens edge and 0.2 mm or more of an interval between lenses.

The program producing the initial solutions uses the optimization method which uses the damping least square method [19], and its algorithm is shown in Fig. 5.

For an 8 element projection lens, by properly applying initial values of 35 variables (really, d_0=260 and c_9=0, so there are 33 variables), and using the damping least square method, the 33 variables are decided in a way that the value of

$$error\ function = ((m_\beta + 0.2924)^2 + (u_k^{pr})^2 + (S_I)^2 + (S_{II})^2 + (S_{III})^2 + (S_{IV})^2 + (S_V)^2)^{\frac{1}{2}} \quad (13)$$

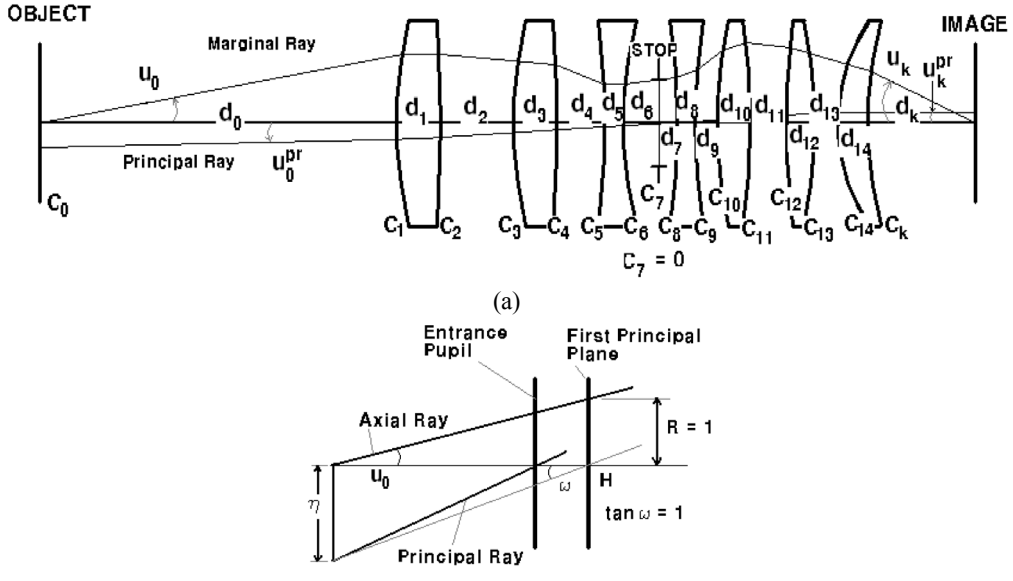

FIG. 4. Schematic diagram of the DMD projection lens system.

becomes 10^{-9} or below. To prevent the solution from being a local minimum, initial solutions were repeatedly obtained by allowing 33 variables to be selected variously within the potentially feasible specific areas. Similarly, initial solutions were calculated for 7 or 6 element projection lenses.

The fifth spherical aberration (Δy) can be calculated by following Eq. (14) [16, 17].

$$\Delta y = -\frac{1}{8u_k} T_I R^5 \tag{1}$$

In this equation, R is the height of the paraxial marginal ray in the entrance pupil.

Eqs. (14) is used for calculating the residual fifth spherical aberration of each initial solution. Here, u_k is given by the ray tracing under the condition of $u_0=\frac{52}{2\times d_0}$. Summarized optical characteristics of the initial solutions gained by these methods are given in Table 3.

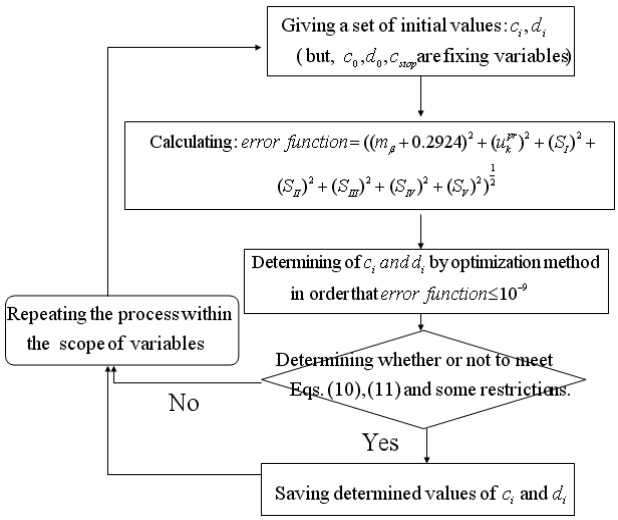

FIG. 5. Flow chart for solving the simultaneous equations of initial DMD projection lens systems.

For the 6 element system, not all of the third-order aberrations can be eliminated and thus this system is not suitable for our purpose.

For the 7 element system, the initial solutions were obtained either when a lens was added to the front of the stop or the back of the stop. As a result, it was confirmed that the third-order aberration was all eliminated for the initial solution and the amount of the residual fifth-order spherical aberration was 0.02 mm or more. In case of the 7 element system mentioned above, It had the residual spherical aberration larger than 20 μm, so it was considered to be a low-profile system that could not give the resolution of below 4 μm, and it was true when we optimized it.

The 8 element system is a system that added two lenses on the front/back in a separated Biotar(DoubleGauss type) lens system, and the distribution of its refraction power is +,+,+,-, (stop), +,-,+,+/ +,+,+,-, (stop), -,+,+,+ and the third-order aberrations are all eliminated and the amount of the residual fifth-order spherical aberration is 0.002 mm or more. Among those initial solutions gained, we selected a proper initial solution for optimization with a consideration of feasibility of fabrication, related data and configurations are given in Table 4 and Fig. 6.

Fig. 7 shows the residual finite ray aberrations of the selected initial solution of which the object numerical aperture (NA) is 0.1($\frac{52}{2\times 260}$=0.1*rad*) and proves that at least 2 or more high-order aberrations are left in the on-axis aberration diagram (Fig. 7(a)) presented the spherical aberration. Because at present the total residual spherical aberration is about 2 μm or less, it is confirmed that there is no need to gain initial numerical solutions by adding lens to further remove high-order spherical aberrations. That is, it is possible to further reduce the marginal aberration value of the residual spherical aberration in the optimization process by combination of the third, fifth, and seventh order spherical aberration, so it is rational to conclude that there is no need to gain numerical solutions by adding more lenses to simultaneously remove the third and fifth order spherical aberration. Fig. 8 shows the astigmatism and distortion of the selected initial solution and proves that the astigmatism and distortion is almost absent for the full field.

TABLE 3. Optical characteristics of the initial numerical solutions

The number of elements	Distribution of Power			3rd aberrations	5th spherical aberration (mm)
	The front	Stop	The rear		
6	+ + +		+ + +	All aberrations can't be zero simultaneously.	>0.14
7	+ + + -		+ + +	All zero	>0.022
	+ + -		- + + +	All zero	>0.020
	+ + -		+ - + +	All zero	>0.022
8	+ + + -		- + + +	All zero	>0.003
	+ + + -		+ - + +	All zero	>0.002

TABLE 4. Design data of the selected initial projection lens solution

Surface	Radius	Thickness	Glass
Object	Infinity	260	
1	105.4975	13.1780	FD8
2	-389.253	20.1018	
3	56.5628	8.0352	FD8
4	80.7580	2.4186	
5	34.6506	13.9739	FD8
6	-265.444	0.4101	
7	-192.609	4.7890	FD8
8	17.1851	10.4716	
Stop	Infinity	3.8089	
10	-24.6043	9.9457	FD8
11	155.0977	2.4322	
12	131.1344	11.9536	FD8
13	-36.2594	19.9554	
14	175.0992	7.0606	FD8
15	-123.028	0.1000	
16	45.6524	11.2937	FD8
17	95.7155	30.0000	
Image	Infinity	0	

FIG. 6. Configuration of the selected initial solution to be optimized.

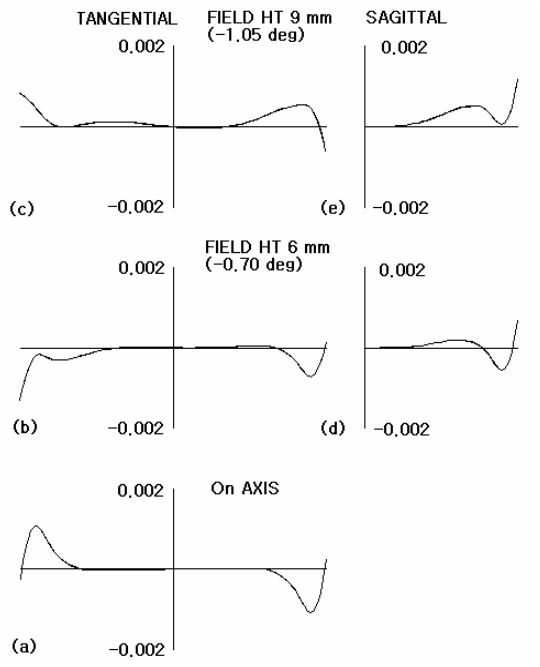

FIG. 7. Finite ray aberration of the selected initial solution. ((a): on-axial ray aberration; (b): tangential ray aberration for 6mm object height; (c): tangential ray aberration for 9 mm object height; (d): sagittal ray aberration for 6 mm object height; (e): sagittal ray aberration for 9 mm object height)

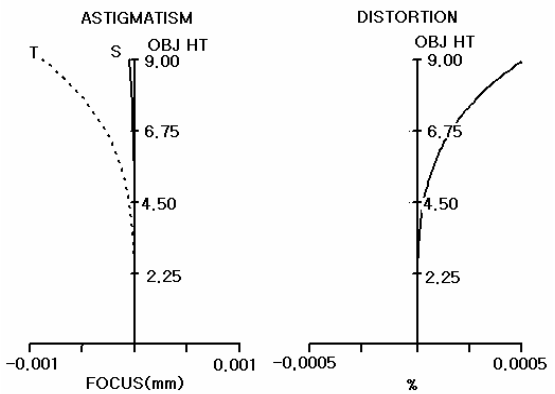

FIG. 8. Astigmatism and Distortion of the selected initial solution.

2.3. Optimized design of projection lens system

We induced and selected an initial solution for the 8 element system in the previous section, and now we have to optimize it to make it consistent with our system.

First of all, we did not consider chromatic aberrations at all while obtaining the initial solution. Therefore, it is necessary to gain the optimized solution with lens material as a variable in the optimization process. In addition, we should perform the optimization process by considering the

TABLE 5. Design data of the optimized projection lens

Surface	Radius	Thickness	Glass
Object	Infinity	260	
1	102.5675	12.0000	734515_OHARA
2	-415.264	19.1396	
3	56.1674	8.0000	734515_OHARA
4	77.6703	2.3721	
5	34.3330	14.0000	691548_SCHOTT
6	-314.612	0.4098	
7	-218.197	5.0000	689312_SCHOTT
8	17.0556	10.91840	
Stop	Infinity	2.5654	
10	-25.0297	10.0000	689312_SCHOTT
11	160.2606	2.4215	
12	116.7647	12.0000	691548_SCHOTT
13	-37.8473	18.4666	
14	194.9924	8.0000	734515_OHARA
15	-113.990	0.5000	
16	43.2567	8.0000	734515_OHARA
17	95.2296	30.0000	
Image	Infinity	0	

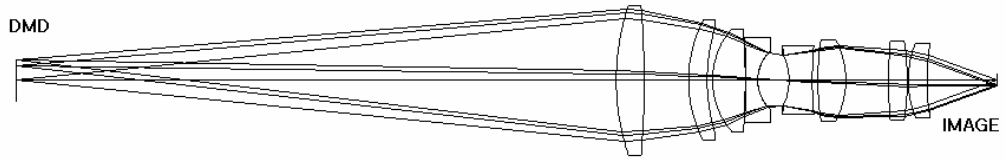

FIG. 9. Configuration of the optimized projection lens.

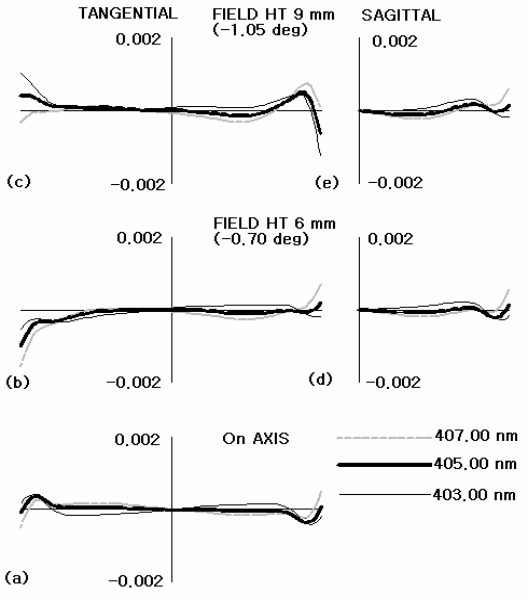

FIG. 10. Finite ray aberrations of the optimized projection lens. ((a): on-axial ray aberration; (b): tangential ray aberration for 6 mm object height; (b): tangential ray aberration for 9 mm object height; (d): sagittal ray aberration for 6 mm object height; (e): sagittal ray aberration for 9 mm object height)

depth of focus of ±1.73 μm on the image surface which is related with the moving precision of the base plate of the user stage and the objective numerical aperture of 0.1.

Table 5 and Fig. 9 show data and configuration of the projection system optimized by the above process. Fig. 9 shows the -0.292× projection system that is able to project mask patterns which are generated by the micromirror of the DMD and exposed on the base plate when the uniform illumination beams are irradiated on the DMD surface and reflected on the micromirror of the DMD. This optical system is designed to maintain the image telecentricity so that to accommodate tiny errors along the optical axis on the base plate of the stage. Since the size of micromirror of DMD is 13.68 μm×13.68 μm, the formed image becomes 4 μm×4 μm. Fig. 10 shows the residual finite ray aberrations of the optimized projection lens and proves that 2 μm or less residual aberrations are left in all of the fields. In particular, Fig. 10(a) shows the residual spherical aberration is 0.5 μm or less. Fig. 11 shows astigmatic and distortion aberrations, indicating that there is almost no distortion within 5.26 mm($|m_\beta|$×18 mm) of a diameter of image field on the substrate. Fig. 12 shows various MTF curves of the optical system. At Fig. 12 (a), (b), (c), we know that the line width of resolution is about 1.14 μm for the depth of focus of ±1.73 μm based on the 50%

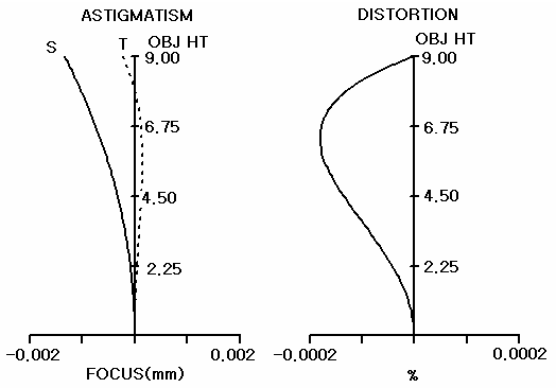

FIG. 11. Astigmatism and distortion of the optimized projection lens.

modulation criterion. In reality, however, the line width would be about 4 μm, taking into account the fabrication tolerances of the lenses and barrel with the barrel structure not using actuators which compensate the distance changes between lenses due to the temperature changes, as showed at Fig. 12 (d), (e), and (f). Hence, the current optical system maintains 4 μm of line width.

III. SYSTEM INTEGRATION AND LITHOGRAPHY EXPERIMENTS

Fig. 13 shows the comprehensive optical system designed so far. The illumination beams from the lamp are reflected by the cold mirror and converged at angles of

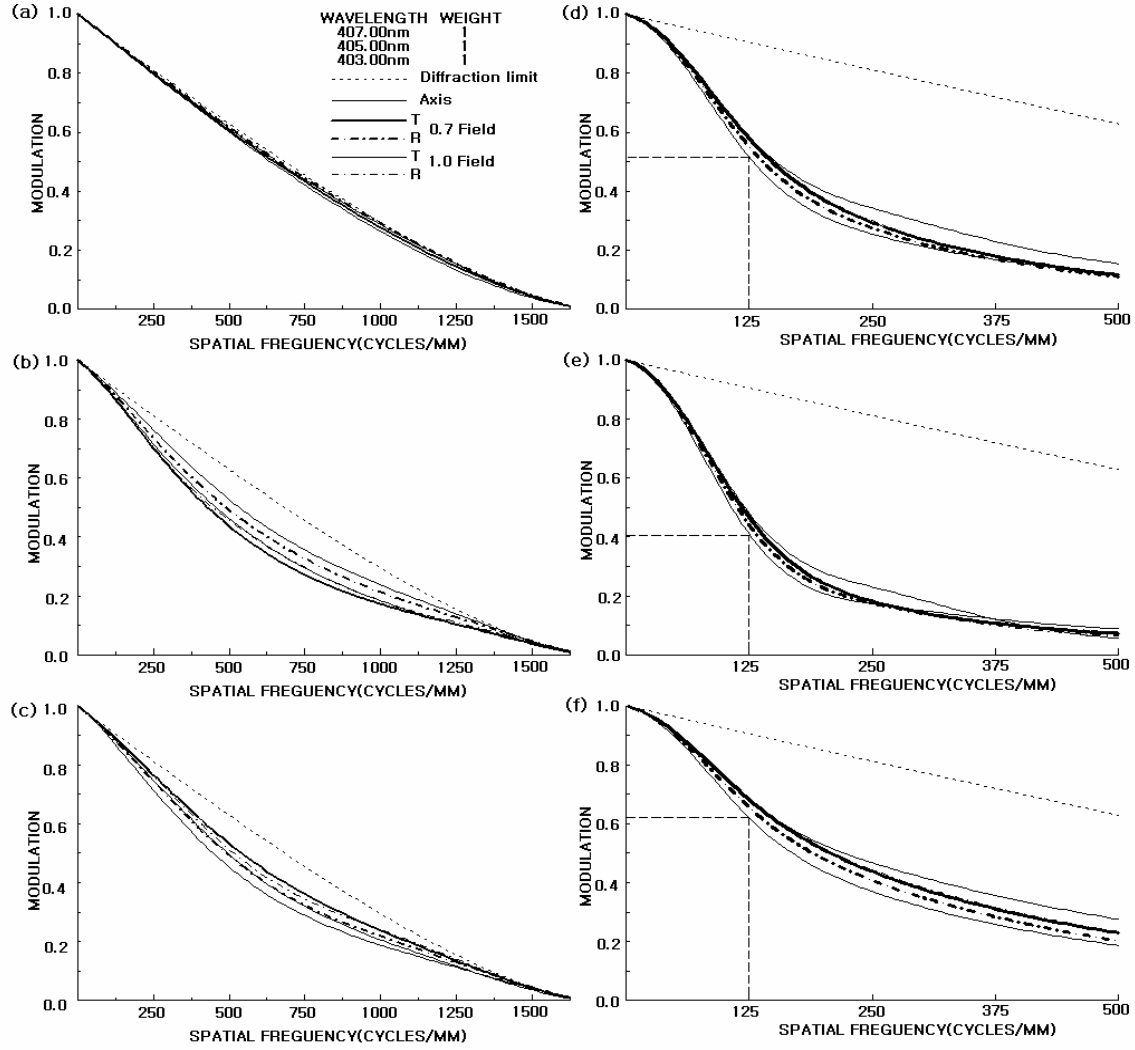

FIG. 12. MTF curves of the optimized projection lens. ((a) : with zero defocusing and no fabrication tolerances; (b) : with defocusing of -1.73 μm and no fabrication tolerances; (c): with defocusing of +1.73 μm and no fabrication tolerances; (d) : with zero defocusing and fabrication tolerances which are distance error of ±0.005 mm, power error of $\frac{\lambda}{8}\sim\frac{\lambda}{4}$, and centering error of 30"~60" ; (e),(f) : with defocusing of ∓ 1.73 μm, respectively, and the same fabrication tolerances mentioned at (d)).

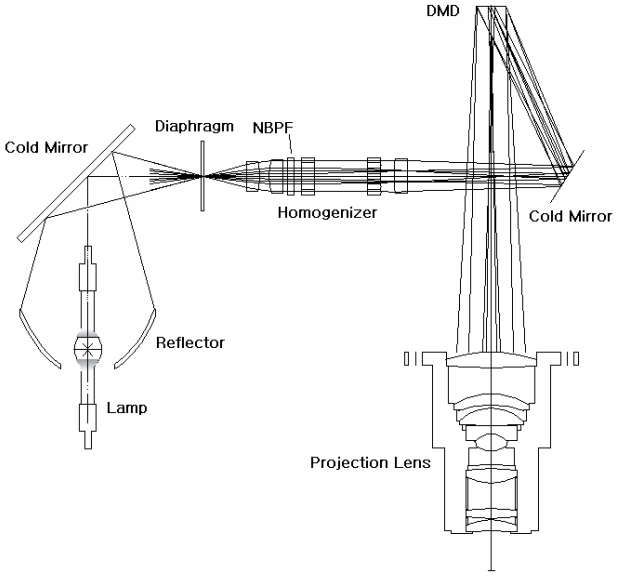

FIG. 13. Integrated maskless lithography optical system.

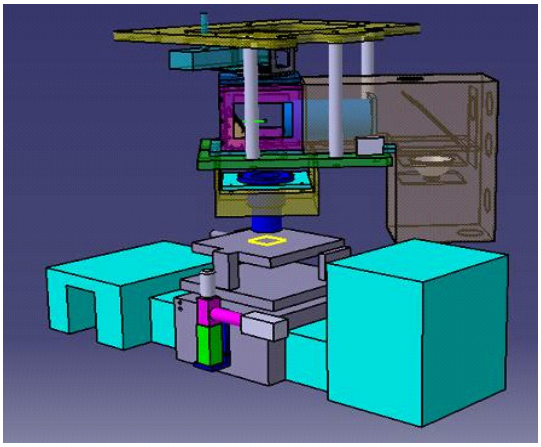

FIG. 14. 3D image of the integrated maskless lithography optical system.

±15°. Then, they pass through a diaphragm and a homogenizer to be reflected by a cold mirror and incident upon the DMD surface. Here, the micromirrors of the DMD reflect the illumination beams in the direction of projection lens according to mask patterns engraved by the pattern generating S/W. In this way, the mask pattern to be implemented is formed upon the substrate on the base plate of the stage. The intensity of illumination beams on the substrate, when all the micromirrors of the DMD reflect the illumination beams toward the optical axis of projection lens, was measured as 230 mW/cm^3.

Fig. 14 shows 3D images of the collection of parts used for fabricating the maskless lithography equipment and Fig. 15 shows the system actually fabricated and installed.

In order to verify the feasibility of the maskless lithographic optical system, lithography experiments were performed using the equipment where the developed optical system is

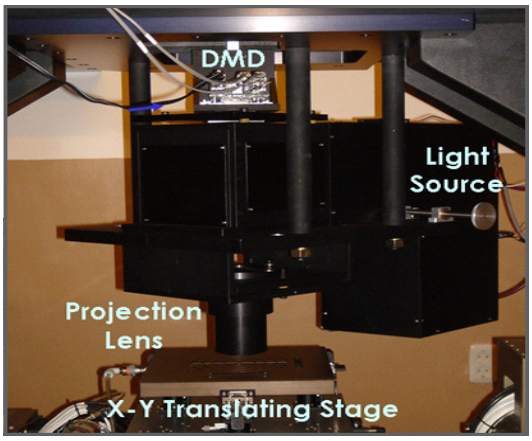

FIG. 15. Close-up photograph of the maskless lithography optical engine.

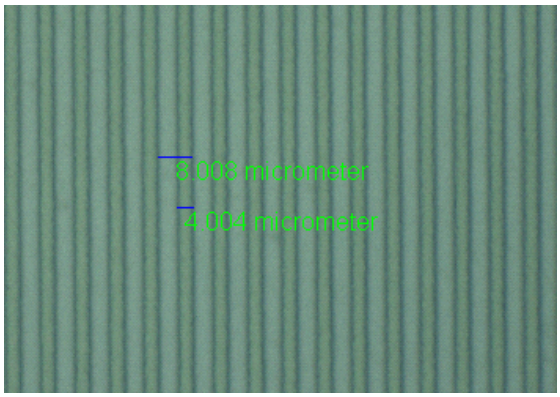

FIG. 16. Image of a pattern exposed by the developed maskless lithography optical system.

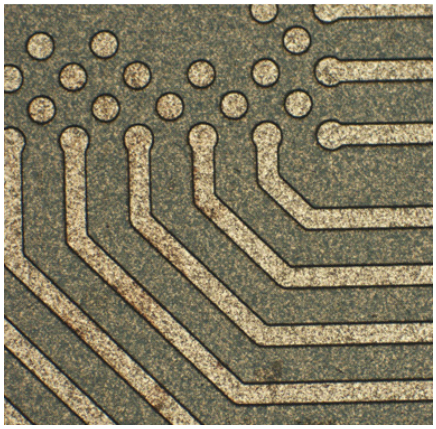

FIG. 17. Microscopic image of a PCB pattern on a flexible substrate made by the developed maskless lithography optical system.

loaded [20]. The lithography result shown in Fig. 16 is 4 μm vertical lines on a wafer and it proves that 4 μm resolution is achieved. Fig. 17 shows a microscopic image

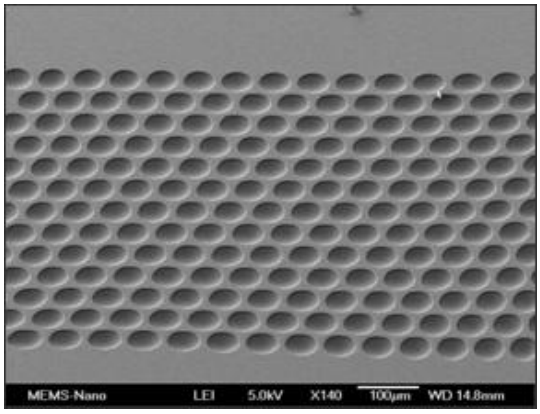

FIG. 18. Electron microscopic image of a mold sample made by the developed maskless lithography optical system, which can be used to make an aspheric MLA.

of a PCB pattern on a flexible substrate and Fig. 18 shows an electron microscopic image of a mold sample made by the developed optic system, by which an aspheric MLA can be fabricated, and in the near future it will be used for development of the maskless lithography using an aspheric MLA.

IV. CONCLUSIONS

We separately designed and fabricated an illumination part, and a projection lens part, and by integrating them, we completed a 4 μm class maskless lithography optical system. This system can be applied to PCB and/or FPD fabrication, and we predict that this system could solve various problems like expense and time in fabricating the masks, contamination by masks, disposal of masks, and the alignment of masks which were major disadvantages of the conventional mask lithography optical system. The proposed system could be verified by lithography experiments which gives the line pattern with the resolution of 4 μm line width. Our future work will mainly focus on the development of the maskless lithography optical system with MLA which is developed by this equipment.

ACKNOWLEDGMENT

The author gives thanks to CEO J. S. Chae (KEO/CVI) for his help in developing the system and Prof. M. Seo and H. Kim (Tongmyong University) for their help throughout the experiments.

REFERENCES

1. D. Dudley, W. Duncan, and J. Slaughter, "Emerging digital micromirror device (DMD) applications," Proc. SPIE **4985**, 14-29 (2003).
2. R. Hofling and E. Ahl, "ALP: universal micromirror controller for metrology and testing," Proc. SPIE **5289**, 322-329 (2004).
3. W. Mei, T. Kanatake, and A. Ishikawa, "Moving exposure system and method for maskless lithography system," U.S. Patent 6,379,867 B1 (2002).
4. W. Mei, "Point array maskless lithography," U.S. Patent 6,473,237 B2 (2002).
5. A. Beeker, W. Cebuhar, J. Kreuzer, A. Latypov, and Y. Vladimirsky, "Methods and systems to compensate for a stitching disturbance of a printed pattern in a maskless lithography system utilizing overlap of exposure zones with attenuation of the aerial image in the overlap region," U.S. Patent 6,876,440 B1 (2005).
6. K. F. Chan, Z. Feng, R. Yang, A. Ishikawa, and W. Mei, "High-resolution maskless lithography," Journal of Microlithography, Microfabrication, and Microsystems **2**, 331-339 (2003).
7. T. Kanatake, "High resolution point array," U.S. Patent 6,870,604 B2 (2005).
8. M. Seo and H. Kim, "Occupancy based pattern generation method for maskless lithography," Patent KR 10-0655165 (2006), Patent Application Pub. No. US/12/095,037 (2008).
9. R. Menon, A. Patel, D. Chao, M. Walsh, and H. Smith, "Zone-plate-array lithography (ZPAL): optical maskless lithography for cost-effective patterning," Proc. SPIE **5751**, 330-339 (2005).
10. G. Seitz, S. Schulte, U. Dinger, O. Hocky, B. Fellner, and M. Rupp, "EUV microlithography: a challenge for optical metrology," Proc. SPIE **5533**, 20-26 (2004).
11. C. Sun, N. Fang, D. Wu, and X. Zhang, "Projection micro-stereolithography using digital micro-mirror dynamic mask," Sens. Actuators A **121**, 113-120 (2005).
12. M. Seo and H. Kim, "Lithography upon micromirrors," Computer Aided Design **39**, 202-217 (2007).
13. W. J. Smith, *Modern Lens Design*, 2nd ed. (McGraw-Hill Professional, New York, USA, 2004), Chapter 12.
14. J. U. Lee and S. M. Yu, "Analytic design procedure of three-mirror telescope corrected for spherical aberration, coma, astigmatism, and Petzval field curvature," J. Opt. Soc. Korea **13**, 184-192 (2009).
15. S. C. Park, S. H. Lee, and J. G. Kim, "Compact zoom lens design for a 5x mobile camera using prism," J. Opt. Soc. Korea **13**, 206-212 (2009).
16. Y. Matsui, *Lens Sekkeiho* (*The Method of Lens Design, witten in Japanese*), 1st ed. (Kyoritsu Publication Inc., Tokyo, Japan, 1972), pp. 70-75.
17. T. Kusakawa, *Lens Kogaku* (*Lens optics, witten in Japanese*), 1st ed. (Tokai Univ. Press, Tokyo, Japan, 1988), pp. 218-259.
18. H. A. Buchdahl, *Optical Aberration Coefficients*, 1st ed. (Dover Publication Inc., New York, USA, 1968).
19. R. W. Daniels, *An Introuction to Numerical Methods and Optimization Techniques*, 1st ed. (North-Holland, New York, USA, 1978), Chapter 8.
20. M. Seo and H. Kim, "Digital photofabrication method and system," in *Proc. 2010 International Symposium on Flexible Automation* (Tokyo, Japan, Jul. 2010), paper OS6.